Supplementary Information for:

Hidden symmetry lowering, nanoscale order-disorder transition and ionic conductivity in $Na_{1/2-x}La_{1/2-x}Ba_{2x}ZrO_3$

Mia J. Brennan,[a] Frederick P. Marlton,[b] Biswaranjan Mohanty,[c] Nicolas Dupré,[d] Bernt Johannessen,[e,f] Maxim Avdeev,[a,g] Gabriel J. Cuello,[h] Siegbert A. Schmid,[a*] Oliver J. Wagstaff,[j] Fredrick Z.T. Yang,[k] Chris D. Ling[a*]

[a]*School of Chemistry, The University of Sydney, Sydney, NSW 2006, Australia*

[b]*Centre for Clean Energy Technology, School of Mathematical and Physical Sciences, Faculty of Science, University of Technology Sydney, Sydney, NSW 2007, Australia*

[c]*Sydney Analytical Core Research Facility, The University of Sydney, Sydney, NSW, 2006, Australia*

[d]*Nantes Université, CNRS, Institut des Matériaux de Nantes Jean Rouxel, IMN, F-44000 Nantes, France*

[e]*Australian Synchrotron, 800 Blackburn Rd, Clayton, VIC 3168, Australia*

[f]*Institute for Superconducting & Electronic Materials (ISEM), Faculty of Engineering and Information Sciences (EIS), University of Wollongong, Wollongong, NSW 2500, Australia*

[g]*Australian Centre for Neutron Scattering, Australian Nuclear Science and Technology Organisation, New Illawarra Road, Lucas Heights, NSW 2234, Australia*

[h]*Institut Laue-Langevin, 71 avenue des Martyrs, 38042 Grenoble Cedex 9, France*

[j]*Department of Chemistry, Durham University, Stockton Road, Durham, DH1 3LE, United Kingdom*

[k]*Chemistry research laboratory, Department of Chemistry, University of Oxford, 12 Mansfield Road, Oxford, United Kingdom*

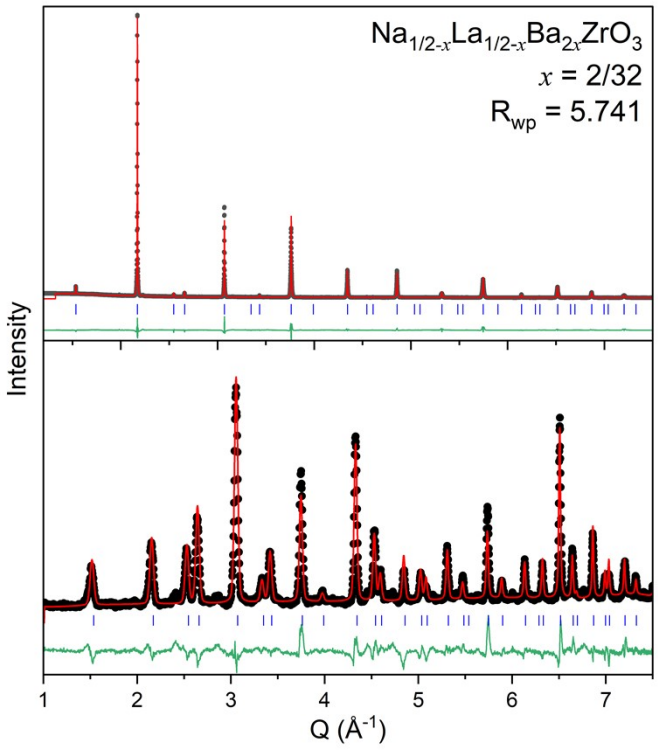

Figure S1: Combined SXRD (upper) and NPD (lower) Rietveld refinement for $Na_{1/2-x}La_{1/2-x}Ba_{2x}ZrO_3$, $x = {}^{2}/_{32}$ to the tetragonal *I*4/*mcm* model in Q-space.

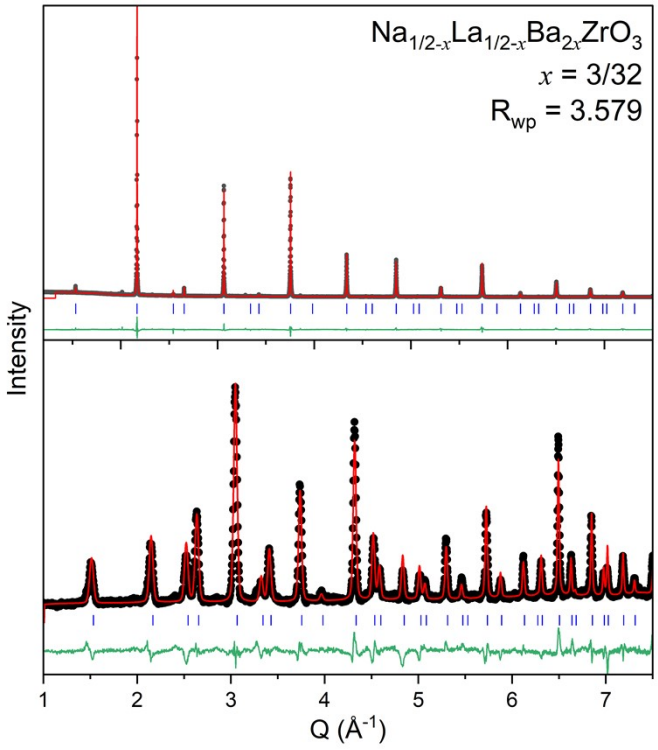

Figure S2: Combined SXRD (upper) and NPD (lower) Rietveld refinement for $Na_{1/2-x}La_{1/2-x}Ba_{2x}ZrO_3$, $x = {}^{3}/_{32}$ to the tetragonal *I*4/*mcm* model in Q-space.

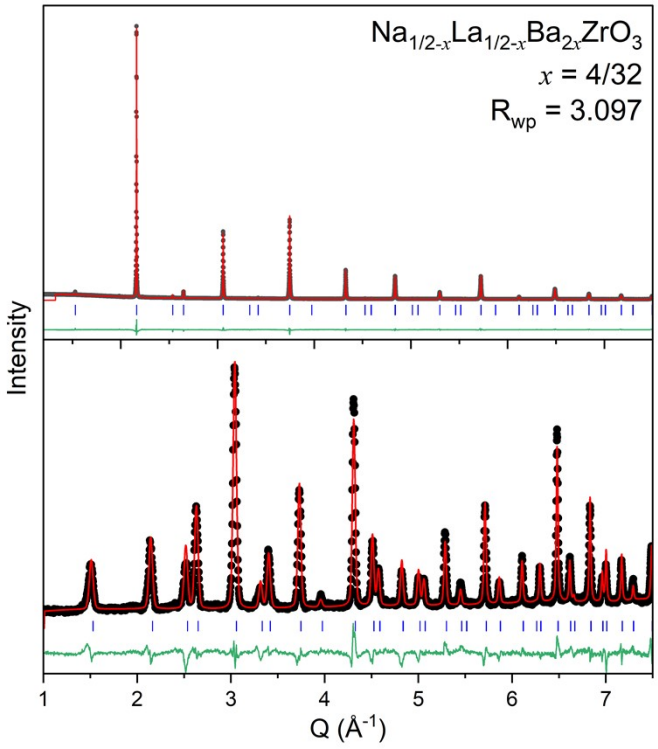

Figure S3: Combined SXRD (upper) and NPD (lower) Rietveld refinement for $Na_{1/2-x}La_{1/2-x}Ba_{2x}ZrO_3$, $x = {}^{4}/_{32}$ to the tetragonal *I*4/*mcm* model in Q-space.

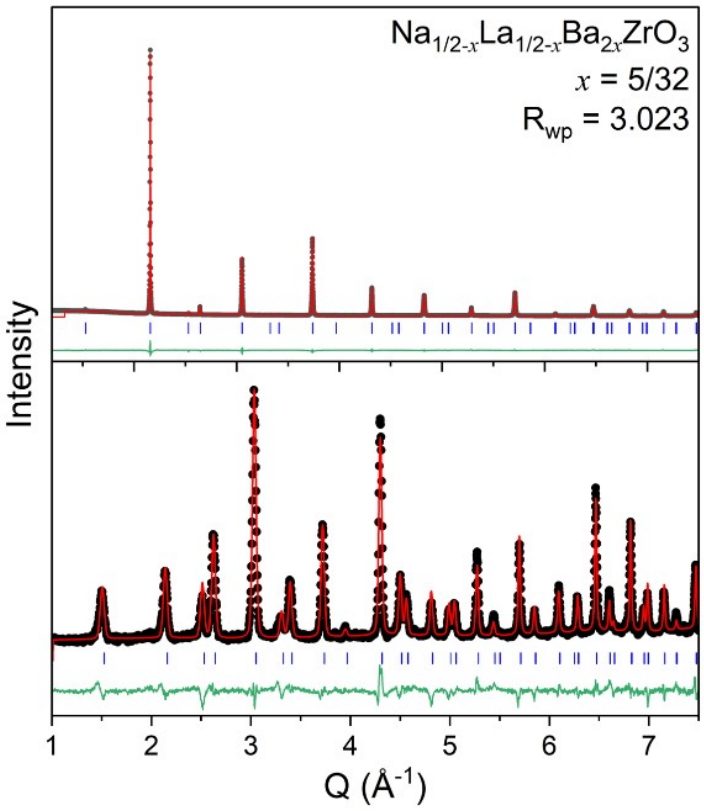

Figure S4: Combined SXRD (upper) and NPD (lower) Rietveld refinement for $Na_{1/2-x}La_{1/2-x}Ba_{2x}ZrO_3$, $x = {}^{5}/_{32}$ to the tetragonal *I*4/*mcm* model in Q-space.

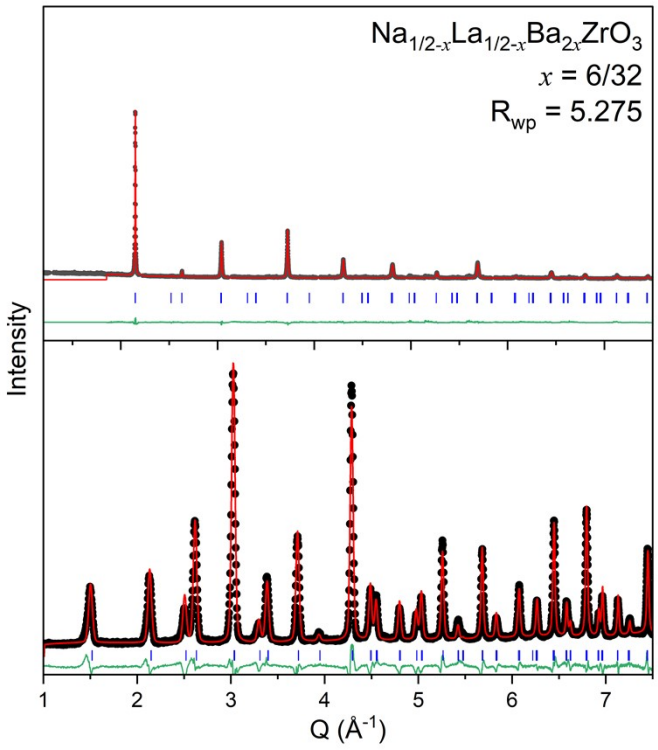

Figure S5: Combined SXRD (upper) and NPD (lower) Rietveld refinement for $Na_{1/2-x}La_{1/2-x}Ba_{2x}ZrO_3$, $x = {}^{6}/_{32}$ to the tetragonal *I*4/*mcm* model in Q-space.

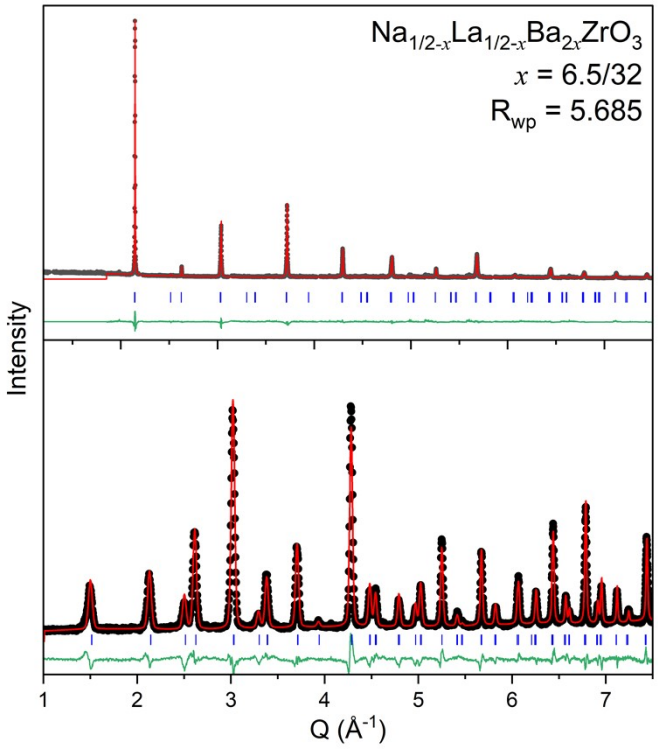

Figure S6: Combined SXRD (upper) and NPD (lower) Rietveld refinement for $Na_{1/2-x}La_{1/2-x}Ba_{2x}ZrO_3$, $x = {}^{6.5}/_{32}$ to the tetragonal *I*4/*mcm* model in Q-space.

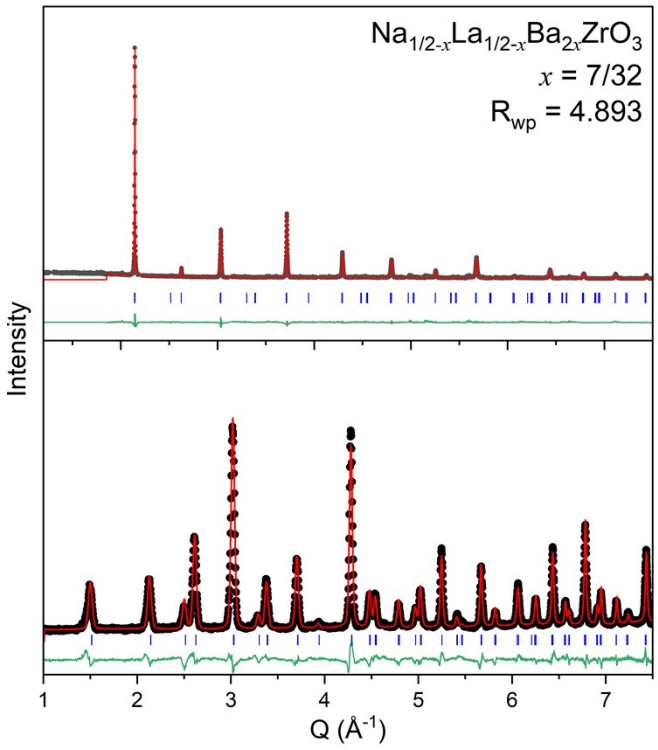

Figure S7: Combined SXRD (upper) and NPD (lower) Rietveld refinement for $Na_{1/2-x}La_{1/2-x}Ba_{2x}ZrO_3$, $x = {}^{7}/_{32}$ to the tetragonal *I*4/*mcm* model in Q-space.

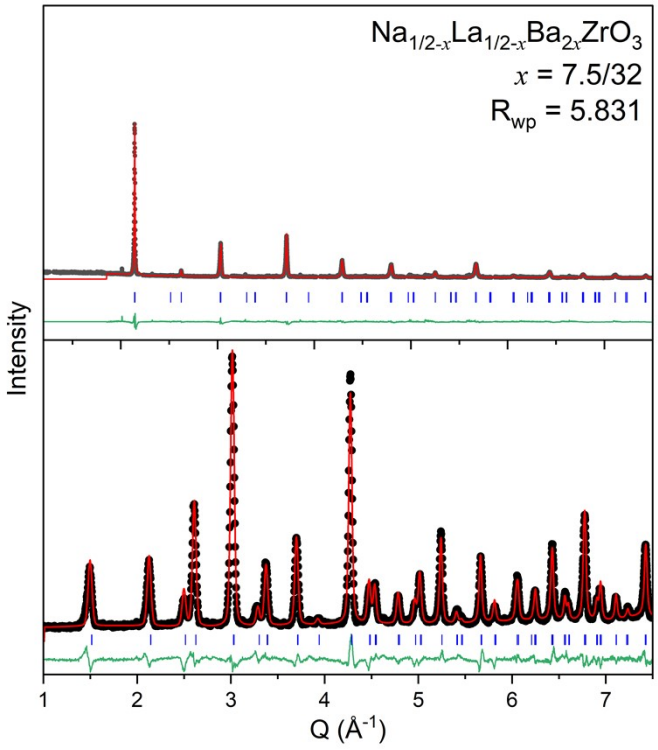

Figure S8: Combined SXRD (upper) and NPD (lower) Rietveld refinement for $Na_{1/2-x}La_{1/2-x}Ba_{2x}ZrO_3$, $x = {}^{7.5}/_{32}$ to the tetragonal *I*4/*mcm* model in Q-space.

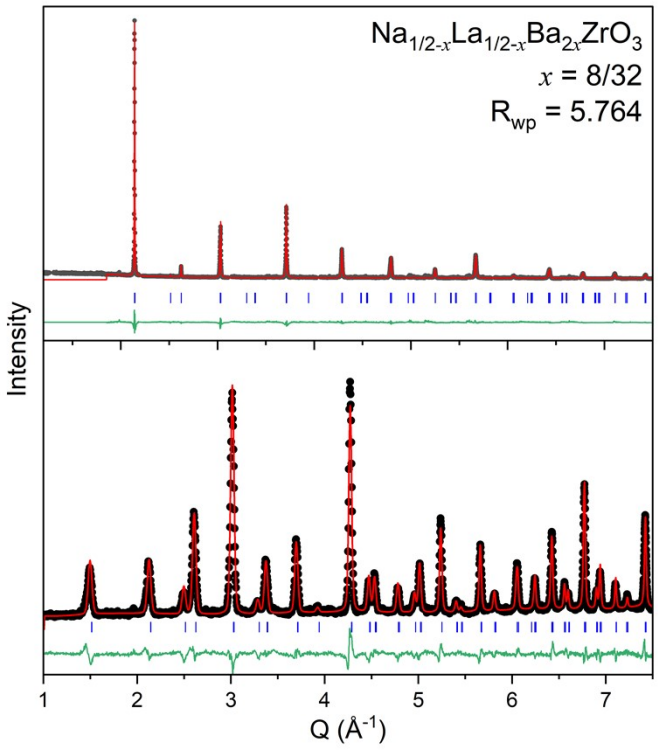

Figure S9: Combined SXRD (upper) and NPD (lower) Rietveld refinement for $Na_{1/2-x}La_{1/2-x}Ba_{2x}ZrO_3$, $x = {}^{8}/_{32}$ to the tetragonal *I*4/*mcm* model in Q-space.

Table S1: Complete combined SXRD (upper) and NPD (lower) Rietveld refinement data for all $Na_{1/2-x}La_{1/2-x}Ba_{2x}ZrO_3$ samples.

Sample *x*	***x* = 2/32**	***x* = 3/32**	***x* = 4/32**	***x* = 5/32**	***x* = 6/32**	***x* = 6.5/32**	***x* = 7/32**	***x* = 7.5/32**	***x* = 8/32**
Space Group	*I*4/*mcm*	*I*4/*mcm*	*I*4/*mcm*	*I*4/*mcm*	*I*4/*mcm*	*I*4/*mcm*	*I*4/*mcm*	*I*4/*mcm*	*I*4/*mcm*
R_{wp} (%)	5.741	3.579	3.079	3.023	5.275	5.685	4.893	5.831	5.764
a (Å)	5.78475(3)	5.79520(3)	5.80693(2)	5.81858(2)	5.83585(4)	5.84498(3)	5.84862(3)	5.85271(7)	5.85719(3)
c (Å)	8.1811(2)	8.19714(5)	8.21746(3)	8.23928(4)	8.27089(9)	8.28236(6)	8.28876(7)	8.30097(14)	8.30149(6)
Volume (Å^3)	273.766(7)	275.296(3)	277.096(2)	278.948(2)	281.683(5)	282.957(4)	283.528(4)	284.343(8)	284.797(4)
Na/La/Ba$_x$	0	0	0	0	0	0	0	0	0
Na/La/Ba$_y$	0.5	0.5	0.5	0.5	0.5	0.5	0.5	0.5	0.5
Na/La/Ba$_z$	0.25	0.25	0.25	0.25	0.25	0.25	0.25	0.25	0.25
U_{11}	0.0000(12)	0.0307(12)	0.0180(11)	0.0165(6)	0.0126(5)	0.0118(7)	0.0122(7)	0.0133(7)	0.0106(8)
U_{33}	0.064(3)	0.0000(16)	0.0000(13)	0.0000(7)	0.0019(8)	0.0052(10)	0.0041(10)	0.0021(11)	0.0075(11)
Zr$_x$	0	0	0	0	0	0	0	0	0
Zr$_y$	0	0	0	0	0	0	0	0	0
Zr$_z$	0	0	0	0	0	0	0	0	0
U_{11}	0.0000(10)	0.0175(10)	0.0211(10)	0.0060(6)	0.0110(6)	0.0072(7)	0.0068(7)	0.0052(7)	0.0068(8)
U_{33}	0.075(2)	0.0000(17)	0.0000(14)	0.0186(8)	0.0091(9)	0.0160(12)	0.0156(11)	0.0146(12)	0.0138(13)
O1$_x$	0	0	0	0	0	0	0	0	0
O1$_y$	0	0	0	0	0	0	0	0	0
O1$_z$	0.25	0.25	0.25	0.25	0.25	0.25	0.25	0.25	0.25
U_{11}	0.047(2)	0.0470(19)	0.0437(12)	0.0399(12)	0.0265(6)	0.0230(8)	0.0208(8)	0.0221(10)	0.0160(9)
U_{33}	0.017(4)	0.034(3)	0.0121(15)	0.0000(14)	0.0000(8)	0.0000(11)	0.0000(11)	0.0000(14)	0.0000(14)
O2$_x$	0.1988(3)	0.2009(2)	0.20125(17)	0.20333(19)	0.20854(12)	0.21076(19)	0.21223(18)	0.21384(19)	0.2147(2)
O2$_y$	0.6988(3)	0.7009(2)	0.70125(17)	0.70333(19)	0.70854(12)	0.71076(19)	0.71223(18)	0.71384(19)	0.7147(2)
O2$_z$	0	0	0	0	0	0	0	0	0
U_{11}	0.0000(7)	0.0032(5)	0.0035(3)	0.0125(4)	0.0115(3)	0.0151(4)	0.0147(4)	0.0153(5)	0.0161(5)
U_{33}	0.108(4)	0.079(2)	0.0798(16)	0.0567(14)	0.0594(9)	0.0544(13)	0.0499(12)	0.0390(12)	0.0471(15)
U_{12}	0.0067(11)	0.0092(11)	0.0095(8)	0.0074(8)	0.0164(5)	0.0151(8)	0.0154(7)	0.0172(8)	0.0143(9)

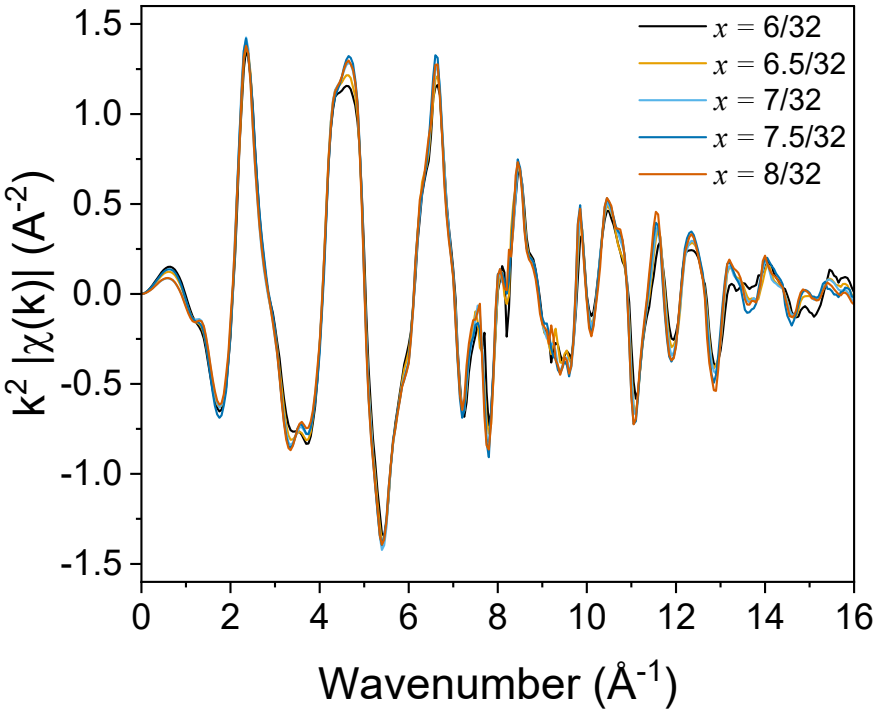

Figure S10: Processed XAFS data of $Na_{1/2-x}La_{1/2-x}Ba_{2x}ZrO_3$ $x = {}^{6}/_{32} - {}^{8}/_{32}$ overlayed in *k*-space from 0.0 – 16.0 Å^{-1}.

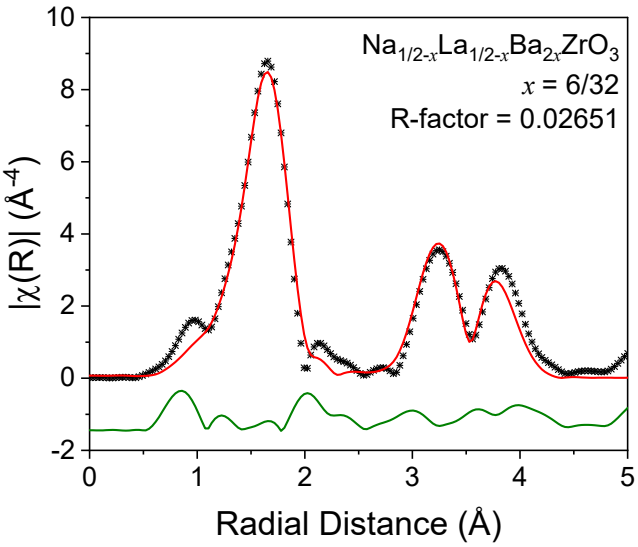

Figure S11: Radial distance plot of the $Na_{1/2-x}La_{1/2-x}Ba_{2x}ZrO_3$, $x = {}^{6}/_{32}$ EXAFS refinement between 1.0 - 4.5 Å.

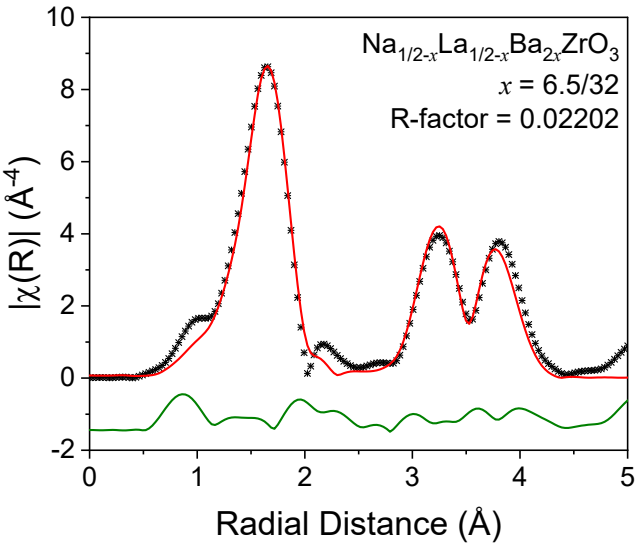

Figure S12: Radial distance plot of the $Na_{1/2-x}La_{1/2-x}Ba_{2x}ZrO_3$, $x = {}^{6.5}/_{32}$ EXAFS refinement between 1.0 - 4.5 Å.

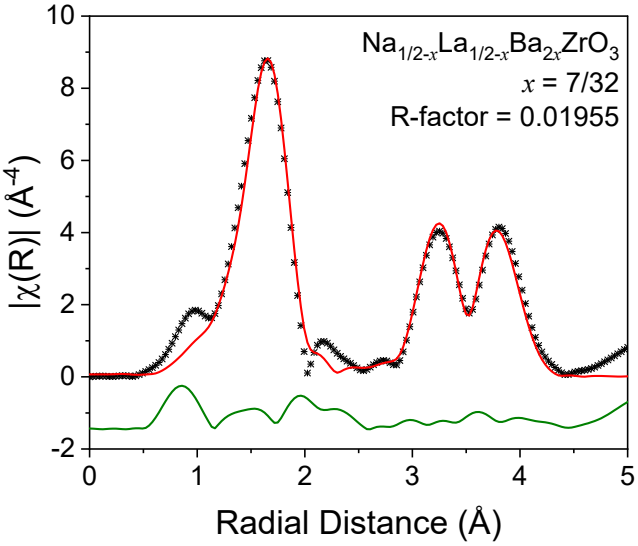

Figure S13: Radial distance plot of the $Na_{1/2-x}La_{1/2-x}Ba_{2x}ZrO_3$, $x = {}^{7}/_{32}$ EXAFS refinement between 1.0 - 4.5 Å.

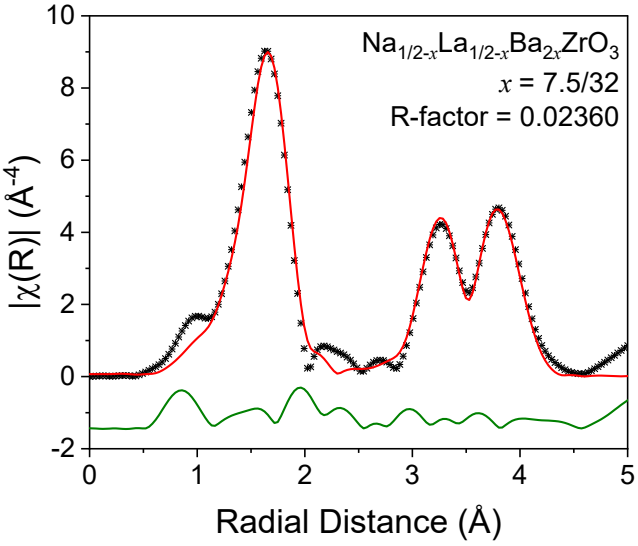

Figure S14: Radial distance plot of the $Na_{1/2-x}La_{1/2-x}Ba_{2x}ZrO_3$, $x = {}^{7.5}/_{32}$ EXAFS refinement between 1.0 - 4.5 Å.

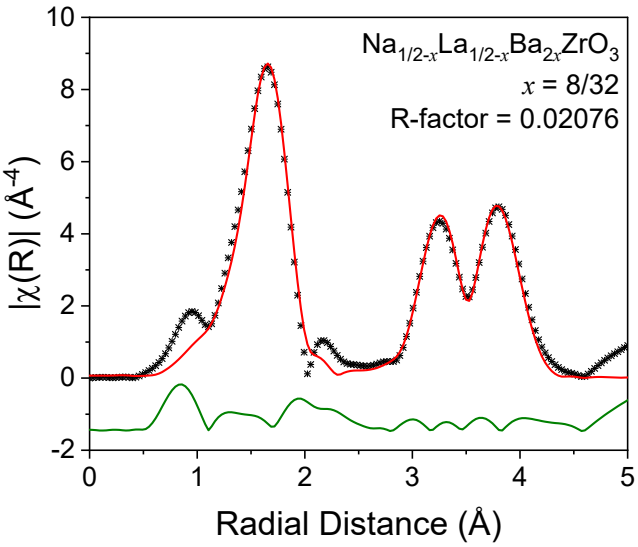

Figure S15: Radial distance plot of the $Na_{1/2-x}La_{1/2-x}Ba_{2x}ZrO_3$, $x = {}^{8}/_{32}$ EXAFS refinement between 1.0 - 4.5 Å.

Table S2: EXAFS scattering paths and associated parameters for $Na_{1/2-x}La_{1/2-x}Ba_{2x}ZrO_3$, $x = {}^{6}/_{32}$.

x = 6/32 ***R factor = 0.02651***

Scattering Path	**Scatter type**	**N**	**S_0^2**	**σ^2**	**ΔE_0**	**ΔR**	**R_{eff}**	**R**
Abs – O – Abs	Single	6	1.021	0.005	-2.548	0.00887	2.0835	2.09237
Abs – A – Abs	Single	3	1.021	0.006	-2.548	0.00844	3.5763	3.58474
Abs – Zr1 – Abs	Single	6	1.021	0.014	-2.548	0.02449	4.1295	4.15399
Abs – O – Zr2 – Abs	Forward	4	1.021	0.010	-2.548	-0.01385	4.1354	4.12155
Abs – O – Zr2 – O1 – Abs	Double forward	2	1.021	0.010	-2.548	-0.01385	4.1354	4.12155
Abs – O – Zr1 – Abs	Forward triangle	8	1.021	0.015	-2.548	0.04979	4.1548	4.20459
Abs – O – Abs – O – Abs	Forward through absorber	4	1.021	0.016	-2.548	0.03365	4.1829	4.21655
Abs – O – Zr1 – O – Abs	Forward Triangle	4	1.021	0.016	-2.548	0.07789	4.1829	4.26079

Table S3: EXAFS scattering paths and associated parameters for $Na_{1/2-x}La_{1/2-x}Ba_{2x}ZrO_3$, $x = {}^{6.5}/_{32}$.

x = 6.5/32 ***R factor = 0.02202***

Scattering Path	**Scatter type**	**N**	**S_0^2**	**σ^2**	**ΔE_0**	**ΔR**	**R_{eff}**	**R**
Abs – O – Abs	Single	6	1.021	0.005	-2.548	0.00936	2.0847	2.09406
Abs – A – Abs	Single	3	1.106	0.005	-2.548	0.01074	3.5817	3.59244
Abs – Zr1 – Abs	Single	6	1.021	0.013	-2.548	0.02602	4.1357	4.16172
Abs – O – Zr2 – Abs	Forward	4	1.021	0.008	-2.548	-0.00948	4.1412	4.13172
Abs – O – Zr2 – O1 – Abs	Double forward	2	1.021	0.008	-2.548	-0.00948	4.1412	4.13172
Abs – O – Zr1 – Abs	Forward triangle	8	1.021	0.014	-2.548	0.04862	4.1583	4.20692
Abs – O – Abs – O – Abs	Forward through absorber	4	1.021	0.016	-2.548	0.03292	4.1836	4.21652
Abs – O – Zr1 – O – Abs	Forward Triangle	4	1.021	0.016	-2.548	0.07392	4.1836	4.25752

Table S4: EXAFS scattering paths and associated parameters for $Na_{1/2-x}La_{1/2-x}Ba_{2x}ZrO_3$, $x = {}^{7}/_{32}$.

x = 7/32 ***R factor = 0.01955***

Scattering Path	**Scatter type**	**N**	**S_0^2**	**σ^2**	**ΔE_0**	**ΔR**	**R_{eff}**	**R**
Abs – O – Abs	Single	6	1.021	0.004	-2.548	0.01006	2.0849	2.09496
Abs – A – Abs	Single	3	1.191	0.006	-2.548	-0.00115	3.5841	3.58295
Abs – Zr1 – Abs	Single	6	1.021	0.014	-2.548	0.00351	4.1385	4.14201
Abs – O – Zr2 – Abs	Forward	4	1.021	0.007	-2.548	-0.00528	4.1444	4.13912
Abs – O – Zr2 – O1 – Abs	Double forward	2	1.021	0.007	-2.548	-0.00528	4.1444	4.13912
Abs – O – Zr1 – Abs	Forward triangle	8	1.021	0.027	-2.548	0.02411	4.1591	4.18321
Abs – O – Abs – O – Abs	Forward through absorber	4	1.021	0.040	-2.548	0.03282	4.1825	4.21532
Abs – O – Zr1 – O – Abs	Forward Triangle	4	1.021	0.040	-2.548	0.04751	4.1825	4.23001

Table S5: EXAFS scattering paths and associated parameters for $Na_{1/2-x}La_{1/2-x}Ba_{2x}ZrO_3$, $x = {}^{7.5}/_{32}$.

x = 7.5/32								***R factor = 0.02360***
Scattering Path	**Scatter type**	**N**	**S_0^2**	**σ^2**	**ΔE_0**	**ΔR**	**R_{eff}**	**R**
Abs – O – Abs	Single	6	1.021	0.004	-2.548	0.00926	2.0856	2.09486
Abs – A – Abs	Single	3	1.276	0.006	-2.548	0.00978	3.5875	3.59728
Abs – Zr1 – Abs	Single	6	1.021	0.013	-2.548	0.02208	4.1425	4.16458
Abs – O – Zr2 – Abs	Forward	4	1.021	0.006	-2.548	-0.00218	4.1505	4.14832
Abs – O – Zr2 – O1 – Abs	Double forward	2	1.021	0.006	-2.548	-0.00218	4.1505	4.14832
Abs – O – Zr1 – Abs	Forward triangle	8	1.021	0.026	-2.548	0.03958	4.16	4.19958
Abs – O – Abs – O – Abs	Forward through absorber	4	1.021	0.038	-2.548	0.02892	4.1816	4.21052
Abs – O – Zr1 – O – Abs	Forward Triangle	4	1.021	0.038	-2.548	0.06118	4.1816	4.24278

Table S6: EXAFS scattering paths and associated parameters for $Na_{1/2-x}La_{1/2-x}Ba_{2x}ZrO_3$, $x = {}^{8}/_{32}$.

x = 8/32								***R factor = 0.02076***
Scattering Path	**Scatter type**	**N**	**S_0^2**	**σ^2**	**ΔE_0**	**ΔR**	**R_{eff}**	**R**
Abs – O – Abs	Single	6	1.021	0.005	-2.548	0.00949	2.086	2.09549
Abs – A – Abs	Single	3	1.361	0.006	-2.548	0.00908	3.5894	3.59848
Abs – Zr1 – Abs	Single	6	1.021	0.012	-2.548	0.01995	4.1447	4.16465
Abs – O – Zr2 – Abs	Forward	4	1.021	0.006	-2.548	-0.00233	4.1507	4.14837
Abs – O – Zr2 – O1 – Abs	Double Forward	2	1.021	0.006	-2.548	-0.00233	4.1507	4.14837
Abs – O – Zr1 – Abs	Forward Triangle	8	1.021	0.017	-2.548	0.03745	4.1622	4.19965
Abs – O – Abs – O – Abs	l					0.02967	4.1827	4.21237
Abs – O – Zr1 – O – Abs	l					0.05795	4.1827	4.24065

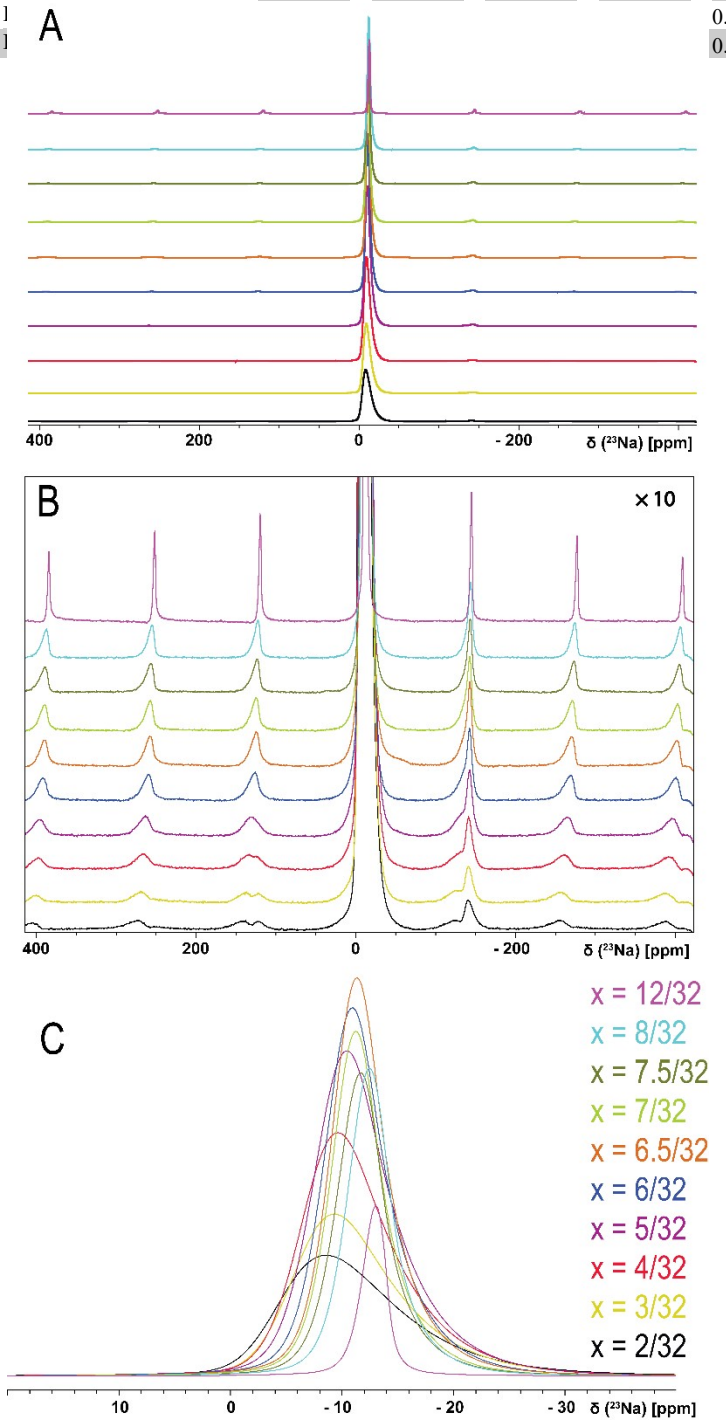

Figure S16: (A) Stacked plot of 1D ^{23}Na MAS spectra as a function of x in $Na_{1/2-x}La_{1/2-x}Ba_{2x}ZrO_3$. (B) The identical spectra are shown in (A). The signals were extended 10-fold to better view the satellite transition sidebands. The asymmetric spinning sideband peak of approximately ± 140 ppm is present in all samples, suggesting sodium is in a less symmetric environment, leading to chemical shift anisotropy. This may be due to the incorporation of bigger barium cations into the lattice, resulting in lattice distortions along crystallographic axes. The centerbands of the central transition are truncated for clarity. (C) Superimposed central transition centerbands of spectra in (A).

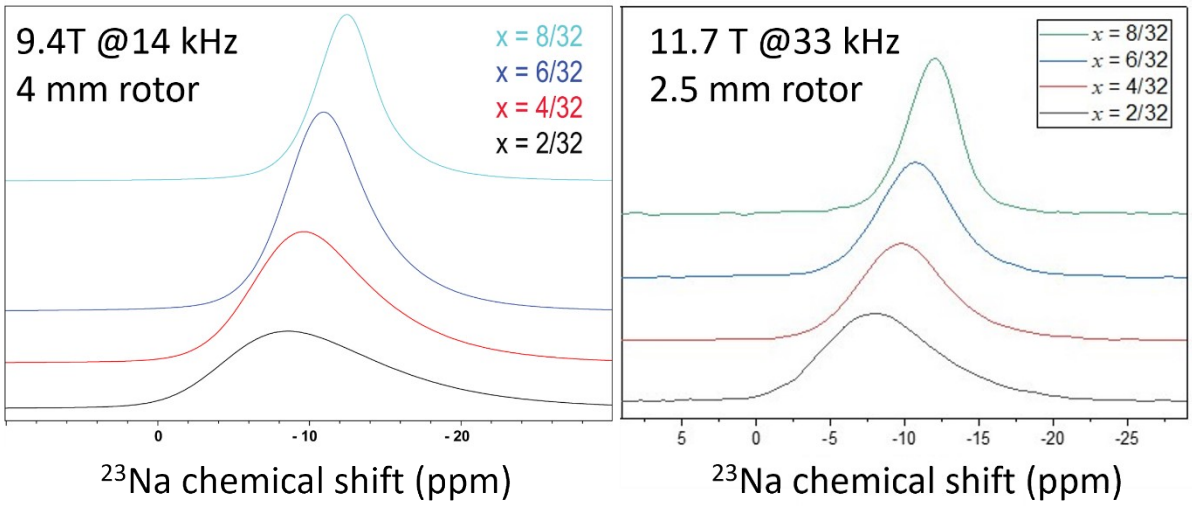

Figure 17: Comparison of the experimental ^{23}Na MAS spectra of $Na_{1/2-x}La_{1/2-x}Ba_{2x}ZrO_3$ at various x at two magnetic fields. The higher field spectra yield narrower lines because the second-order quadrupolar interaction is inversely proportional to the magnetic field strength.

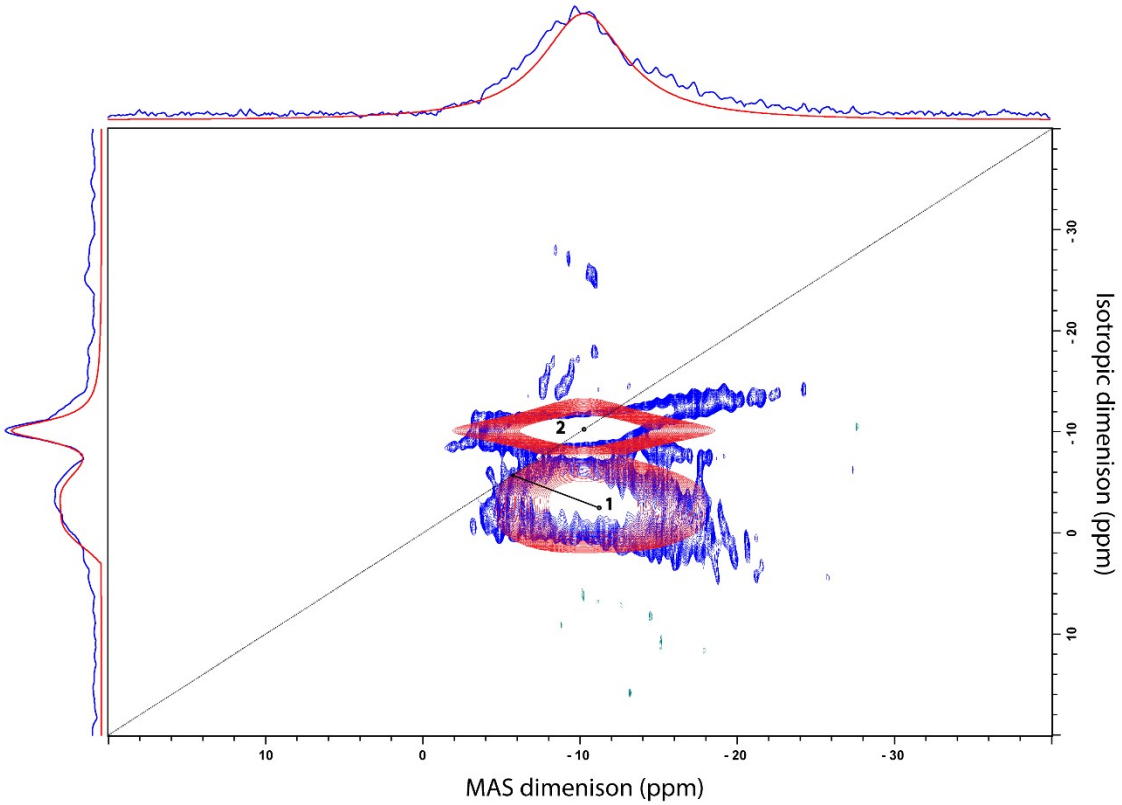

Figure S18: ^{23}Na MQMAS experimental spectrum of $Na_{1/2-x}La_{1/2-x}Ba_{2x}ZrO_3$ ($x = 2/32$). The data was collected on a Bruker AVANCE III 400WB spectrometer (^{23}Na transmitter frequency of 105.8 MHz) with a Bruker CPMAS probe at a sample spinning frequency of 14 kHz. The data was fitted using the sola2d/mqmas routine in Topspin. The two sodium sites are indicated as 1 and 2. The obtained isotropic chemical shift (δ_{iso}), asymmetry parameter (η), and the quadrupolar coupling constant (C_Q) for site 1 from the fitting are -5.7 ppm, 0.25, and 1550 kHz, respectively. For site 2, the isotropic chemical shift (δ_{iso}), asymmetry (η), and C_Q from the fitting are -10 ppm, 0, and 64 kHz, respectively.

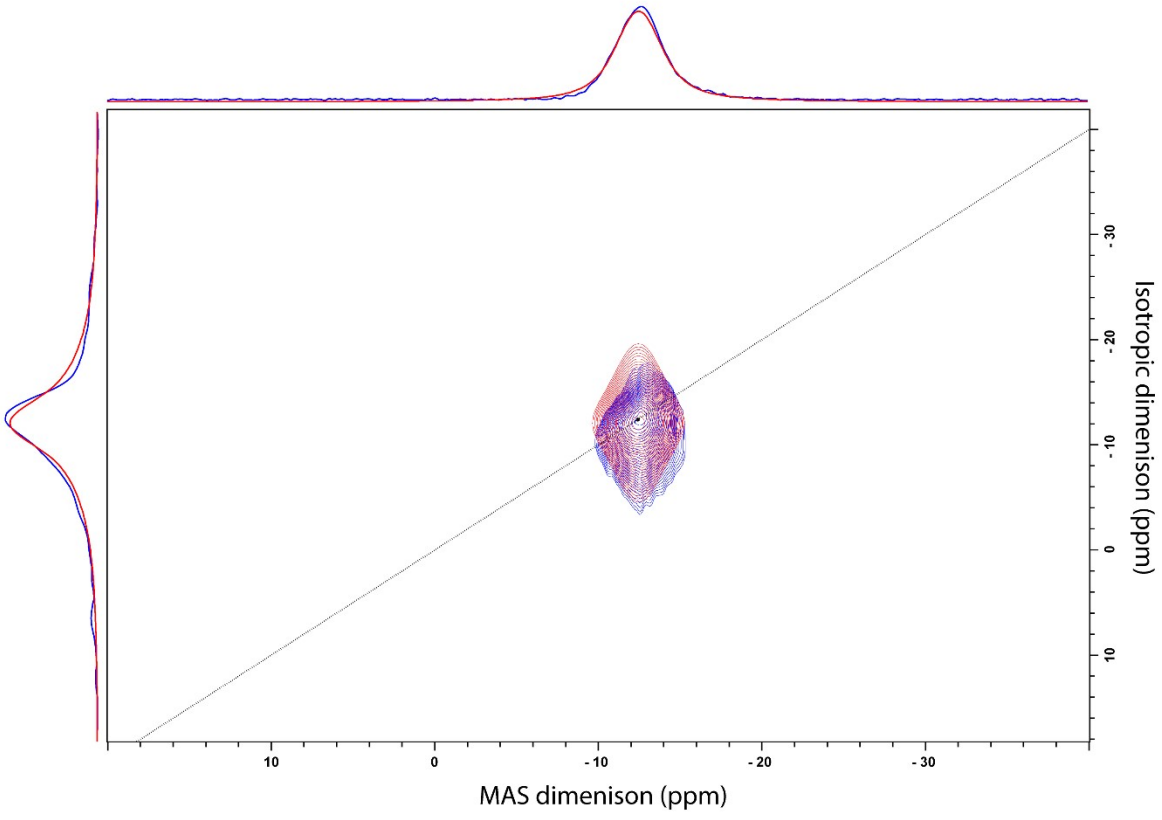

Figure S19: ^{23}Na MQMAS experimental spectrum of $Na_{1/2-x}La_{1/2-x}Ba_{2x}ZrO_3$ ($x = 8/32$). The data was collected on a Bruker AVANCE III 400WB spectrometer (^{23}Na transmitter frequency of 105.8 MHz) with a Bruker CPMAS probe at a sample spinning frequency

of 14 kHz. The data was fitted using the sola2d/mqmas routine in Topspin. In contrast to the sample $Na_{1/2-x}La_{1/2-x}Ba_{2x}ZrO_3$ (x =2/32), a single site was observed in this sample. The obtained isotropic chemical shift (δ_{iso}), asymmetry parameter (η), and the quadrupolar coupling constant (C_Q) for this site from the fitting are -12.4 ppm, 0, and 55 kHz, respectively.

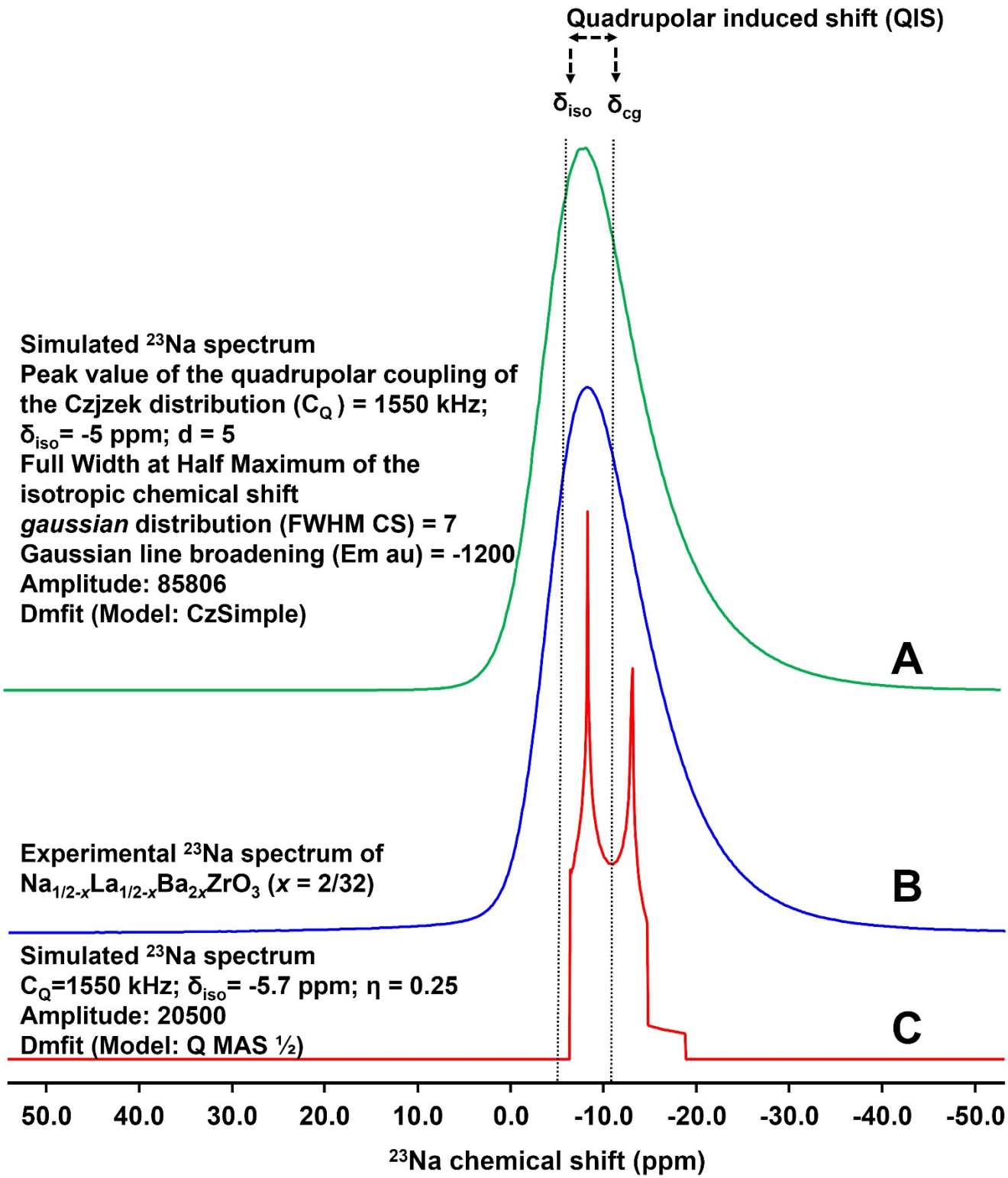

Figure S20: The experimental ^{23}Na spectrum of $Na_{1/2-x}La_{1/2-x}Ba_{2x}ZrO_3$ (x = 2/32) was compared against simulated spectra using Dmfit. For the Dmfit simulation, the isotropic chemical shift (δ_{iso}), asymmetry parameter (η), and the quadrupolar coupling constant (C_Q) obtained for sites 1 and 2 from SOLA were used as initial constraints. a) Simulated spectrum using the CzSimple model. The Czjzek model was applied because it has been extensively used to simulate NMR spectra of crystalline and non-crystalline materials with a high degree of local disorder.(1) b) Experimental spectrum and c) Simulated spectrum using Q MAS ½ model. No Gaussian line broadening was applied. Including the second site's quadrupolar interaction parameters, such as CQ of 64 kHz from SOLA, did not influence the fit. Vertical lines indicate the isotropic chemical shift (δ_{iso}) and the centre of gravity (δ_{cg}).

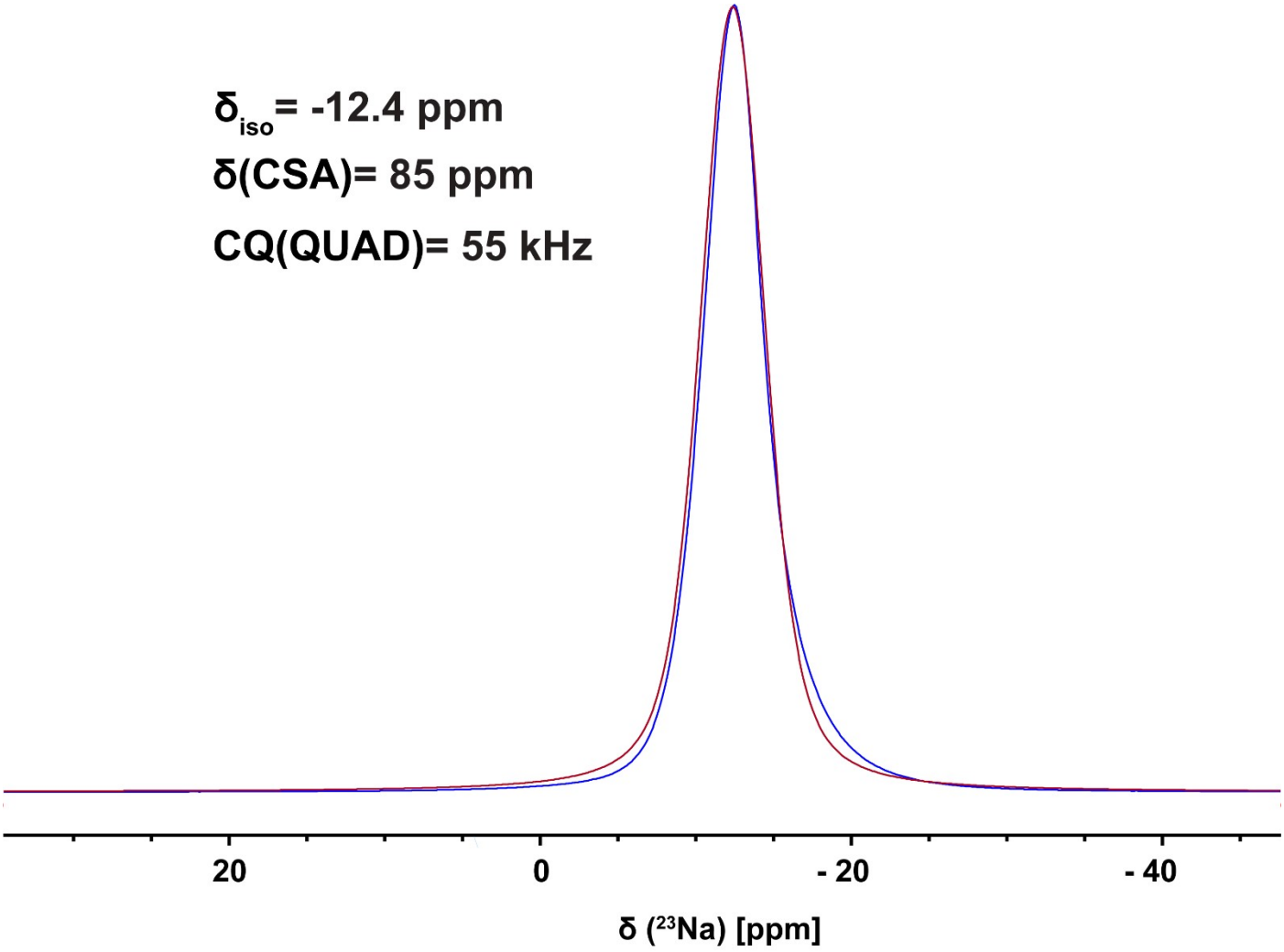

Figure S21: The experimental (blue) and simulated (magenta) ^{23}Na spectra of $Na_{1/2-x}La_{1/2-x}Ba_{2x}ZrO_3$ (x = $^{8}/_{32}$). The spectrum was simulated using QUAD+CSA model in SOLA (Topspin4.4). To fit the 1D ^{23}Na spectrum, the isotropic chemical shift (δ_{iso}) and the quadrupolar coupling constant (C_Q) values obtained from SOLA2D MQMAS fitting were used as constraints. A Lorenzian and Gaussian line broadening of 210 Hz and 390 Hz was applied for fitting.

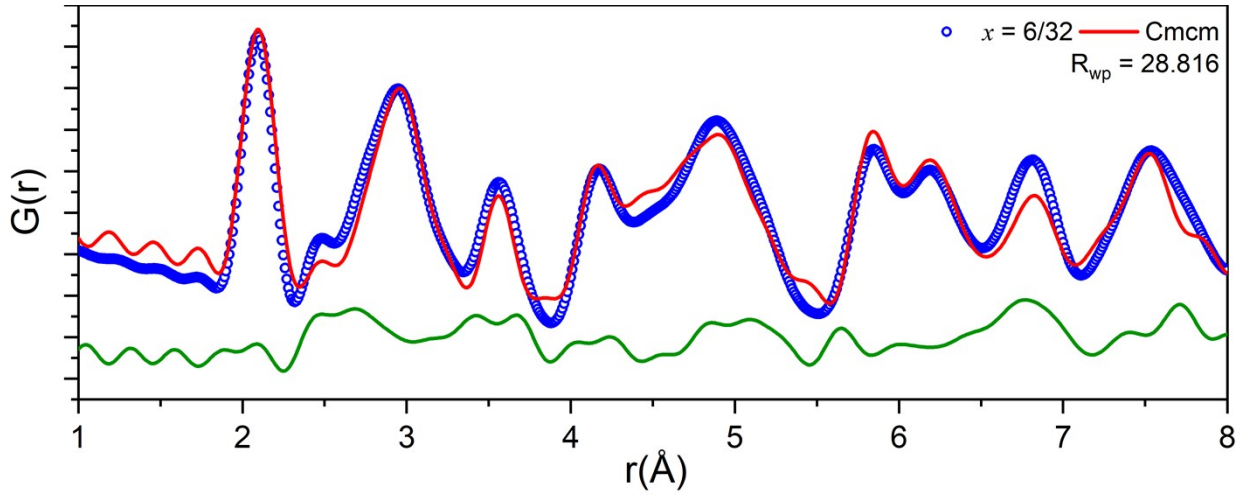

Figure S22: Small box modelling with the orthorhombic *Cmcm* structure against the neutron PDF data of $Na_{1/2-x}La_{1/2-x}Ba_{2x}ZrO_3$, x = $^{6}/_{32}$.

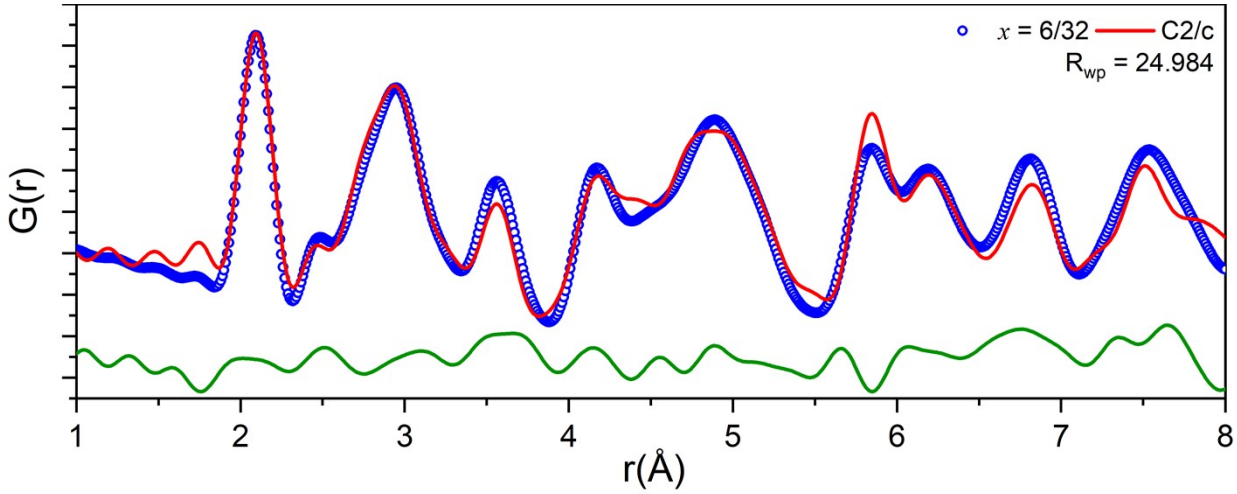

Figure S23: Small box modelling with the monoclinic *C2/c* structure against the neutron PDF data of $Na_{1/2-x}La_{1/2-x}Ba_{2x}ZrO_3$, $x = {}^{6}/_{32}$.

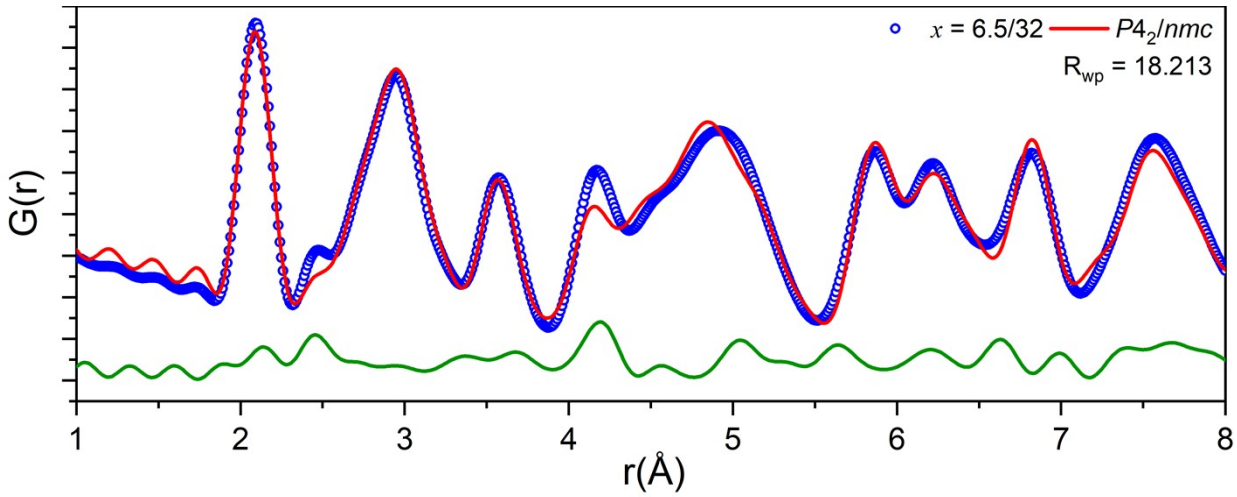

Figure S24: Small box modelling with the orthorhombic $P4_2/nmc$ structure against the neutron PDF data of $Na_{1/2-x}La_{1/2-x}Ba_{2x}ZrO_3$, $x = {}^{6.5}/_{32}$.

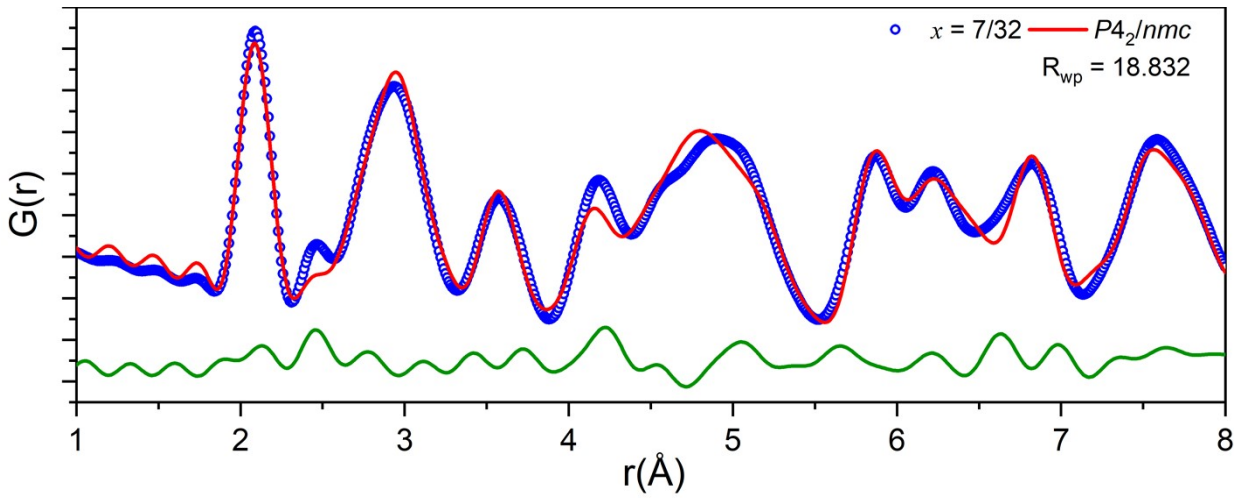

Figure S25: Small box modelling with the orthorhombic $P4_2/nmc$ structure against the neutron PDF data of $Na_{1/2-x}La_{1/2-x}Ba_{2x}ZrO_3$, $x = {}^{7}/_{32}$.

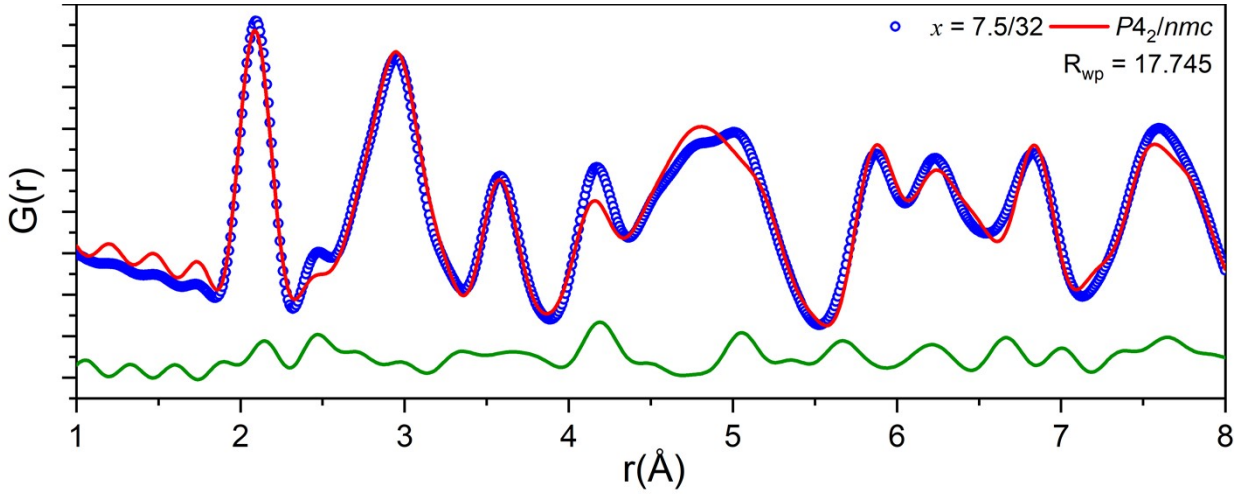

Figure S26: Small box modelling with the orthorhombic $P4_2/nmc$ structure against the neutron PDF data of $Na_{1/2-x}La_{1/2-x}Ba_{2x}ZrO_3$, $x = {}^{7.5}/_{32}$.

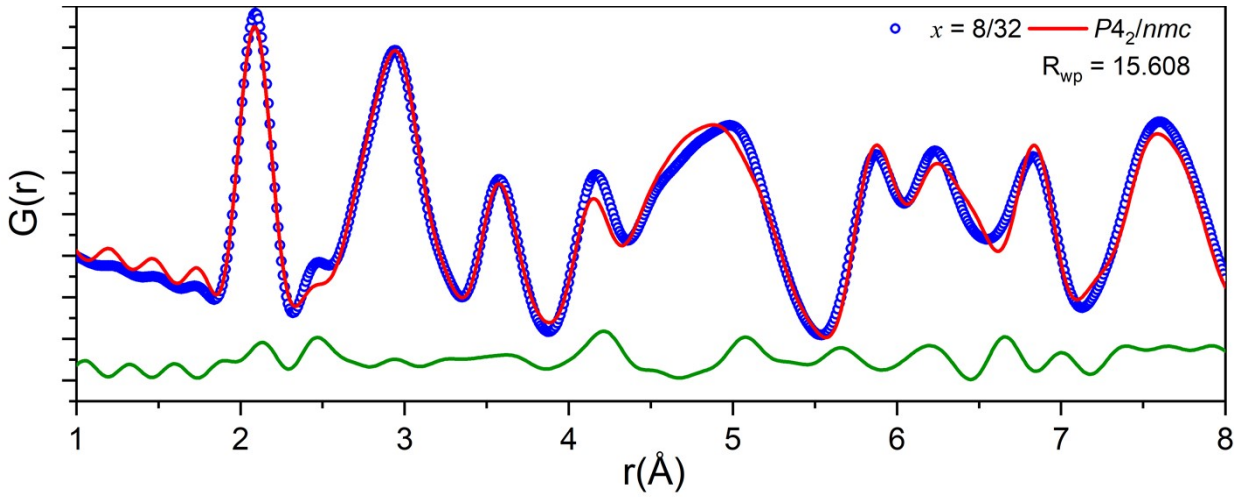

Figure S27: Small box modelling with the orthorhombic $P4_2/nmc$ structure against the neutron PDF data of $Na_{1/2-x}La_{1/2-x}Ba_{2x}ZrO_3$, $x = {}^{8}/_{32}$.

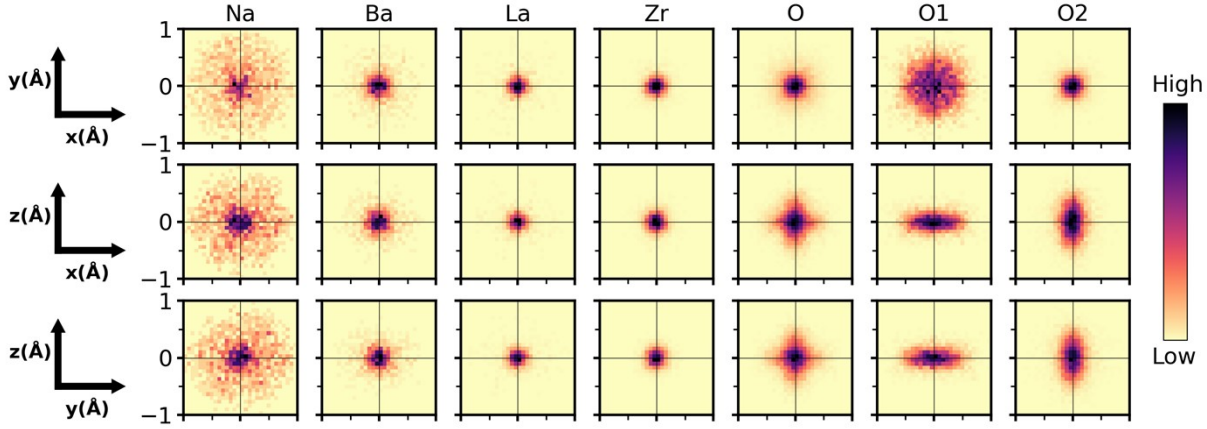

Figure S28: Cumulative 2D probability distributions viewed down each orthogonal axis for the *A*, *B* and O sites in the RMC model of $Na_{1/2-x}La_{1/2-x}Ba_{2x}ZrO_3$ for $x = {}^{6}/_{32}$. The displacement of each atom is calculated relative to the initial input configuration. The *A* site has been split into the constituent elements. The O site has been split into the O1 and O2 sites from the *I*4/*mcm* model. The intensity of the color scale in each plot is normalized to itself.

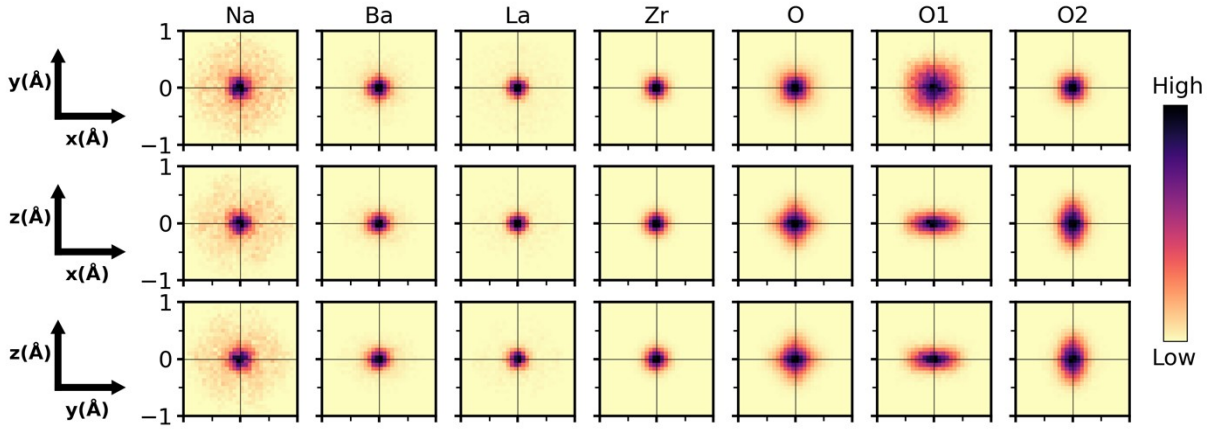

Figure S29: Cumulative 2D probability distributions viewed down each orthogonal axis for the *A, B* and O sites in the RMC model of $Na_{1/2-x}La_{1/2-x}Ba_{2x}ZrO_3$ for $x = {}^{6.5}/_{32}$. The displacement of each atom is calculated relative to the initial input configuration. The *A* site has been split into the constituent elements. The O site has been split into the O1 and O2 sites from the *I*4/*mcm* model. The intensity of the color scale in each plot is normalized to itself.

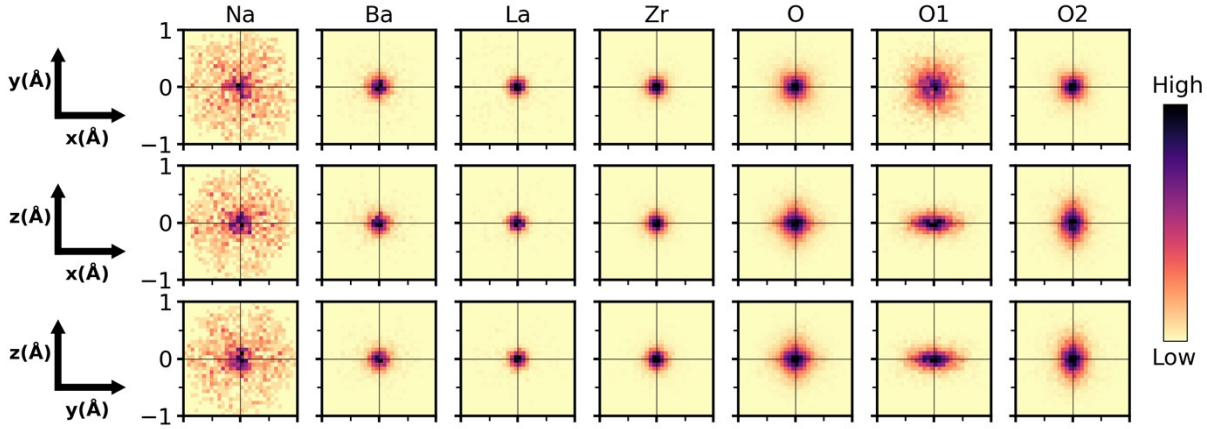

Figure S30: Cumulative 2D probability distributions viewed down each orthogonal axis for the *A, B* and O sites in the RMC model of $Na_{1/2-x}La_{1/2-x}Ba_{2x}ZrO_3$ for $x = {}^{7}/_{32}$. The displacement of each atom is calculated relative to the initial input configuration. The *A* site has been split into the constituent elements. The O site has been split into the O1 and O2 sites from the *I*4/*mcm* model. The intensity of the color scale in each plot is normalized to itself.

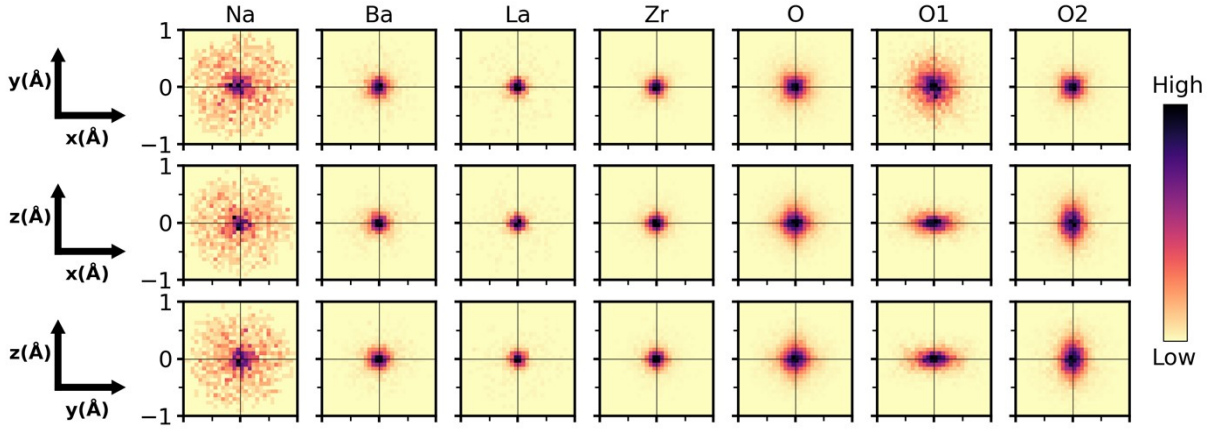

Figure S31: Cumulative 2D probability distributions viewed down each orthogonal axis for the *A, B* and O sites in the RMC model of $Na_{1/2-x}La_{1/2-x}Ba_{2x}ZrO_3$ for $x = {}^{7.5}/_{32}$. The displacement of each atom is calculated relative to the initial input configuration. The *A* site has been split into the constituent elements. The O site has been split into the O1 and O2 sites from the *I*4/*mcm* model.

The intensity of the color scale in each plot is normalized to itself.

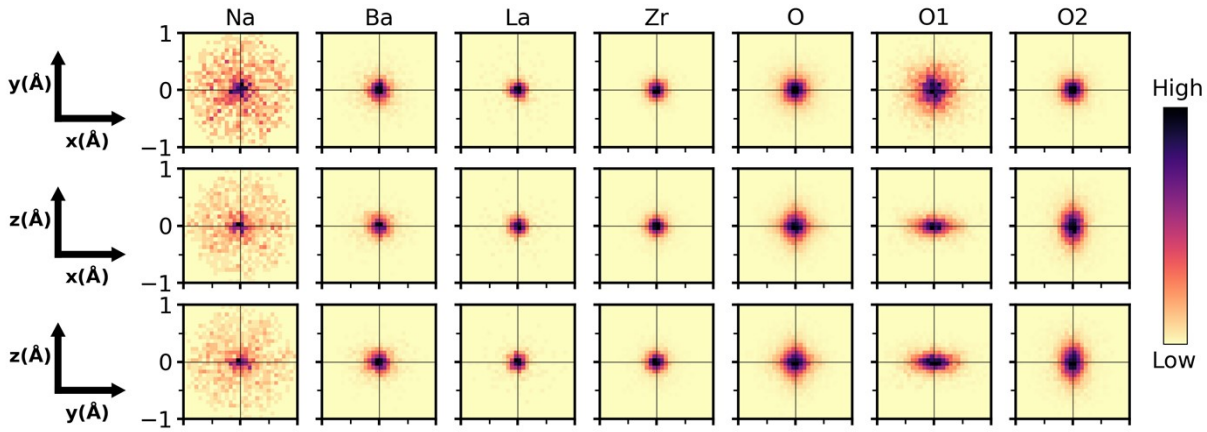

Figure S32: Cumulative 2D probability distributions viewed down each orthogonal axis for the *A, B* and O sites in the RMC model of $Na_{1/2-x}La_{1/2-x}Ba_{2x}ZrO_3$ for $x = {}^{8}/_{32}$. The displacement of each atom is calculated relative to the initial input configuration. The *A* site has been split into the constituent elements. The O site has been split into the O1 and O2 sites from the *I*4/*mcm* model. The intensity of the color scale in each plot is normalized to itself.

Reference

1. d'Espinose de Lacaillerie J-B, Fretigny C, Massiot D. MAS NMR spectra of quadrupolar nuclei in disordered solids: The Czjzek model. Journal of Magnetic Resonance. 2008;192(2):244-51.